Int. J. Sci. R. Tech., 2026 3(5)
A Multidisciplinary peer-reviewed Journal
www.ijsrtjournal.com [ISSN: 2394-7063]

Original Article

Bidirectional Power Converter Topologies For V2G And G2V Integration In Smart Grid Systems: Design, Control, And Performance Evaluation

Poornima S. Kamkar*[1], Sreenath K.[1], H. A. Shruti[1], Chandan N. J.[2], Pradeep N.[2]

[1]*Dept. Of EEE, SSIT Tumkur, Karnataka, India*
[2]*Dept. Of EEE, GPT Tumkur, Karnataka, India*

ABSTRACT

The global energy transition towards renewable sources and electric vehicles (EVs) necessitates robust bidirectional power management between vehicles and the grid. This paper presents the design, modeling, and simulation of bidirectional power converter topologies for Vehicle-to-Grid (V2G) and Grid-to-Vehicle (G2V) applications using MATLAB/Simulink. A Phase-Locked Loop (PLL)-based control strategy is implemented to autonomously regulate bidirectional power flow between EV batteries and the utility grid. Multiple converter topologies are evaluated, including a three-phase full-bridge converter, PWM inverter, DC-DC converters for Light-Duty Vehicles (LDV) and Heavy-Duty Vehicles (HDV), and a complete autonomous V2G-G2V switching system with parallel battery operation. Results demonstrate that the designed system achieves Total Harmonic Distortion (THD) of 2.45% for single-battery operation and 0.93% for parallel battery operation, both well within the IEEE 519 standard limit of 5%. The proposed system confirms the feasibility of smart grid integration with improved efficiency, reliability, and harmonic compliance, while supporting renewable energy integration through effective battery energy management.

Keywords: Vehicle-to-Grid (V2G); Grid-to-Vehicle (G2V); Bidirectional Converter; Phase-Locked Loop (PLL); Total Harmonic Distortion (THD); Smart Grid; Electric Vehicles; MATLAB/Simulink.

INTRODUCTION

The rapid proliferation of electric vehicles (EVs) and the increasing integration of renewable energy sources (RES) have created both challenges and opportunities for modern power grid management. Vehicle-to-Grid (V2G) and Grid-to-Vehicle (G2V) technologies offer a transformative approach, enabling bidirectional energy exchange between EV batteries and the utility grid. When properly implemented within a smart grid framework, these technologies can significantly enhance grid stability, reliability, and efficiency [1,2].

The global EV fleet is expected to grow exponentially over the coming decade, with projections suggesting hundreds of millions of EVs on the road by 2030. The aggregated battery storage capacity of such a fleet represents an enormous distributed energy resource that, if properly harnessed, could address key challenges associated with the intermittent nature of solar and wind power [3,4]. Personal EVs remain parked for an average of 22 hours per day, making them ideal candidates for grid-support services during periods of peak demand or excess renewable generation [5].

However, realizing the full potential of V2G/G2V requires overcoming significant technical hurdles. These include developing efficient bidirectional power converters capable of operating seamlessly in both charging (G2V) and discharging (V2G) modes, implementing robust control strategies that maintain power quality, and ensuring compliance with grid standards such as IEEE 519-1992 for harmonic distortion [6,7]. The converter must also provide power factor correction, harmonic reduction, and proper synchronization with the grid through phase-locking mechanisms [8].

This paper addresses these challenges by presenting a comprehensive design and simulation study of

Relevant conflicts of interest/financial disclosures: The authors declare that the research was conducted in the absence of any commercial or financial relationships that could be construed as a potential conflict of interest.

bidirectional power converter topologies for V2G and G2V applications. The primary contributions include: (i) design and simulation of multiple converter topologies suitable for different EV categories, (ii) development of a PLL-based autonomous control strategy for seamless mode switching, (iii) implementation of parallel battery operation to improve power capacity and harmonic performance, and (iv) validation of harmonic compliance against IEEE standards through FFT analysis.

2. LITERATURE REVIEW

Extensive research has been conducted in recent years on bidirectional EV charger topologies and control strategies. Zhang et al. [1] proposed a power decoupling control for V2G/G2V/PV2G operation modes in a single-phase PV/battery hybrid energy system, demonstrating effective active and reactive power regulation with reduced DC-link capacitance requirements. Their approach reduced capacitor stress by 40% compared to conventional designs.

Islam et al. [2] developed an ANFIS controller-based bidirectional power management scheme for plug-in EVs integrated with the electric grid, showing superior dynamic response compared to conventional PI controllers. The adaptive neuro-fuzzy approach demonstrated particular advantages during transient conditions and mode transitions. Chelladurai et al. [3] presented an interval Type-2 fuzzy logic controlled shunt converter coupled with a novel high-quality charging scheme for EVs, achieving unity power factor operation and THD below 3%.

The challenge of second-order ripple minimization in single-phase on-board chargers was addressed by Seth and Singh [4], who proposed a topology achieving over 98% efficiency. Chen and Huang [5] developed an integrated G2V/V2G switched reluctance motor drive with sensing only switch-bus current, reducing hardware complexity while maintaining robust bidirectional operation. Hosseini et al. [6] introduced an extendable quadratic bidirectional DC-DC converter specifically designed for V2G and G2V applications, capable of achieving high voltage gains with reduced component stress.

Verma and Singh [7] proposed an AFF-SOGI-DRC controlled renewable energy based grid interactive charging station demonstrating significant power quality improvements. Research on inductive power transfer for EVs was advanced by Kao et al. [8], who developed an adaptive bidirectional inductive power and data transmission system. Inala et al. [9] investigated the impact of V2G communication on grid node voltage at charging stations in smart grid scenarios, highlighting the importance of coordinated charging management.

Guru Kumar and Kumaravel [10] presented a dual-input non-isolated DC-DC converter with V2G functionality. Heydari-doostabad and O'Donnell [11] designed a wide-range high-voltage-gain bidirectional DC-DC converter for hybrid EV chargers, achieving a voltage conversion ratio exceeding 10:1. Khalid and Peng [13] analyzed in-cell variation effects on vehicle batteries during V2G bidirectional charging operations, providing important insights for battery management system design. Taghizadeh et al. [14] proposed a multifunctional single-phase EV on-board charger with vehicle-to-vehicle (V2V) charging assistance, while Liu et al. [15] developed a hierarchical V2G/G2V energy management system for electric-drive-reconstructed onboard converters.

Despite significant advances, gaps remain in the literature regarding autonomous mode switching without manual intervention, THD performance under parallel multi-EV operation, and comprehensive comparison of topologies spanning both LDV and HDV categories within a unified simulation framework. This paper addresses these gaps.

3. PROPOSED METHODOLOGY

3.1 System Architecture Overview

The proposed V2G/G2V system consists of three primary stages: (i) a three-phase bidirectional AC/DC converter interfacing with the utility grid, (ii) a bidirectional DC/DC converter regulating the DC bus voltage to match battery requirements, and (iii) a PLL-based control unit that autonomously manages power flow direction and magnitude. Figure 1 illustrates the overall system architecture.

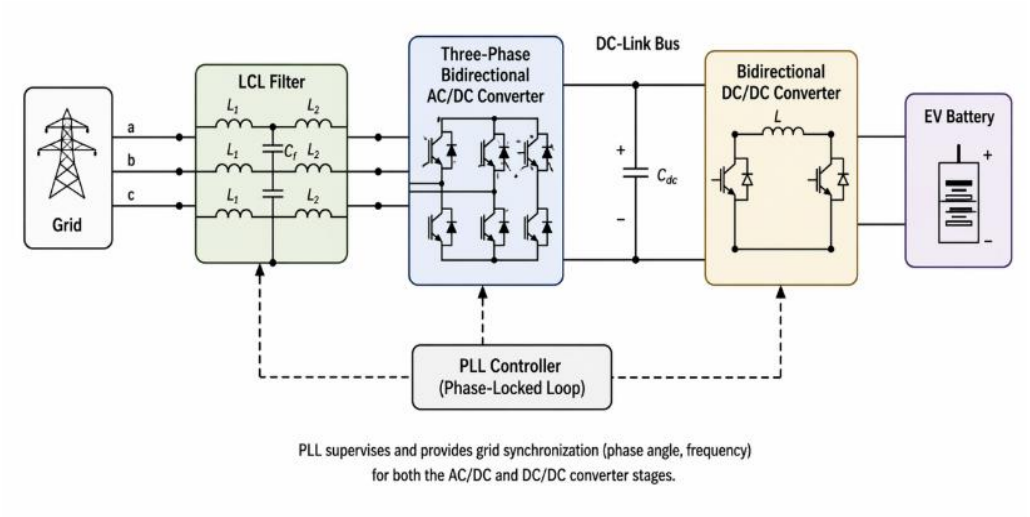

Figure 1: Overall V2G/G2V System Architecture

The system supports both on-board and off-board charging configurations. For Light-Duty Vehicles (LDV), a 3.3 kW two-quadrant full-bridge DC/DC converter is employed, while Heavy-Duty Vehicles (HDV) utilize a 22 kW topology incorporating a three-phase rectifier coupled with a type-C chopper. The control strategy is unified across both configurations through the PLL framework.

3.2 Mathematical Modeling of Key Converters

The three-phase full-bridge (6-pulse) converter forms the core AC/DC interface. The average DC output voltage is expressed as:

$$V_{dc} = \frac{3\sqrt{3}}{\pi} V_m \cos(\alpha) \quad (1)$$

where V_m is the peak phase voltage and α is the firing angle. The normalized average output voltage is given by:

$$V_n = \frac{V_{dc}}{V_{dm}} = cos(\alpha) \quad (2)$$

For the boost converter stage, the relationship between input and output voltage is derived from inductor volt-second balance:

$$V_{out} = \frac{V_{in}}{1-D} \quad (3)$$

where D is the duty cycle. The required inductance to limit current ripple Δi_L is:

$$L = \frac{V_s D}{\Delta i_L f_s} \quad (4)$$

For the PLL voltage controller, the park transformation converts three-phase voltages to the rotating dq0 reference frame:

$$\begin{bmatrix} V_d \\ V_q \end{bmatrix} = \frac{2}{3} \begin{bmatrix} \cos\theta & \cos\left(\theta - \frac{2\pi}{3}\right) & \cos\left(\theta + \frac{2\pi}{3}\right) \\ -\sin\theta & -\sin\left(\theta - \frac{2\pi}{3}\right) & -\sin\left(\theta + \frac{2\pi}{3}\right) \end{bmatrix} \begin{bmatrix} V_a \\ V_b \\ V_c \end{bmatrix} \quad (5)$$

3.3 PLL-Based Control Strategy

The Phase-Locked Loop (PLL) controller constitutes the central control mechanism. It synchronizes the converter switching patterns with the grid voltage and determines the direction of power flow. The voltage controller transforms the measured three-phase grid voltages through Clarke and Park transformations into the dq0 reference frame. The condition Vq = 0 is enforced via a PI controller (Kp = 10, Ki = 50000) to achieve phase lock, generating the angular frequency output ωt.

The current controller maintains DC-link voltage at 800V reference by generating an active current reference Id_ref through an outer PI controller (Kp = 0.5, Ki = 5). An inner current PI controller (Kp = 25, Ki = 500) processes the d-axis current error to produce the modulation index md. Reactive power control maintains Iq_ref = 0 to ensure unity power factor operation during active power transfer.

For V2G mode, the battery current reference is set to +30 A (discharging), resulting in positive active

power injection into the grid with voltage and current in phase. For G2V mode, the reference switches to -30 A (charging), reversing the power flow with a 180° phase shift between grid voltage and current. Figure 2 shows the PLL control block diagram.

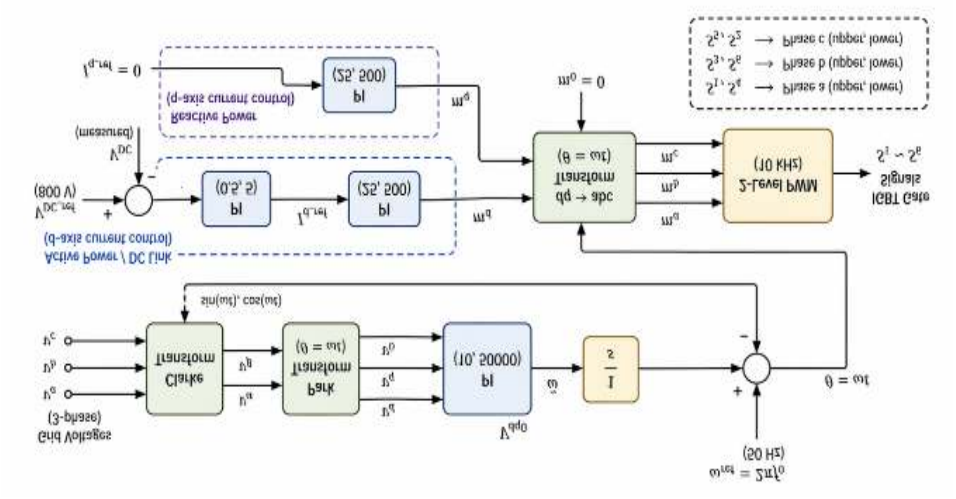

Figure 2: PLL Control Block Diagram for Bidirectional Power Flow

3.4 Battery Charging and Discharging Controller

The battery management controller monitors the actual battery current (Ibat) and compares it with the reference value through a PI controller (Kp = 0.005, Ki = 10) with an output limiter of (0, 0.95). The controller output drives the PWM DC-DC converter at 10 kHz, generating complementary gate signals for the buck and boost MOSFETs. This ensures CC-CV charging compliance and prevents overcharge conditions. The controller seamlessly handles abrupt mode transitions, with the PLL re-synchronizing within approximately 50 ms.

3.5 Parallel Battery Operation

To simulate multi-EV grid interaction, a parallel battery configuration is implemented whereby multiple battery packs share the common DC-link bus. Each battery unit is connected through an independent DC/DC converter subsystem controlled by the same reference current. This architecture increases the system's power capacity proportionally while also improving harmonic performance due to the effective increase in switching frequency seen by the grid filter.

4. RESULTS AND DISCUSSION

4.1 Three-Phase Full Bridge Converter Performance

The three-phase fully controlled full-wave bridge converter (6-pulse) was simulated with a firing angle α = 90° on a 415 V (line-to-line), 50 Hz supply feeding a 10 Ω resistive load. As shown in Figure 3, the simulation confirms the expected rectified output waveform with six pulses per cycle. At α = 90°, the average DC output voltage approaches zero, demonstrating the rectifier's controllable nature across the full range from maximum rectification (α = 0°) to inversion (α > 90°).

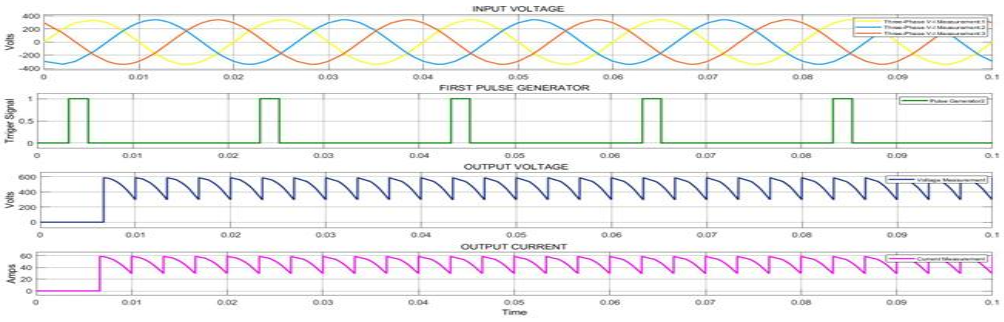

Figure 3: Three-Phase Full Bridge Converter Waveforms at α = 90°

Four-panel plot showing: (top) Three-phase input voltages Va, Vb, Vc (±400V, 50Hz); (second) Pulse generator trigger signal for thyristor T1; (third) Output DC voltage waveform showing 6-pulse ripple (~0-600V); (bottom) Output current waveform (~0-60A) — all plotted over 0 to 0.1 seconds

4.2 Three-Phase PWM Inverter

The three-phase sine-PWM bridge inverter was tested with a 100 V DC source and 10 Ω resistive load, employing a sawtooth carrier at 1 kHz against a 50 Hz sinusoidal modulating signal. Figure 4 presents the input control signal and the resulting output phase and line voltages. The PWM switching effectively shapes the output to approximate a sinusoidal waveform, with harmonic content concentrated around the switching frequency multiples.

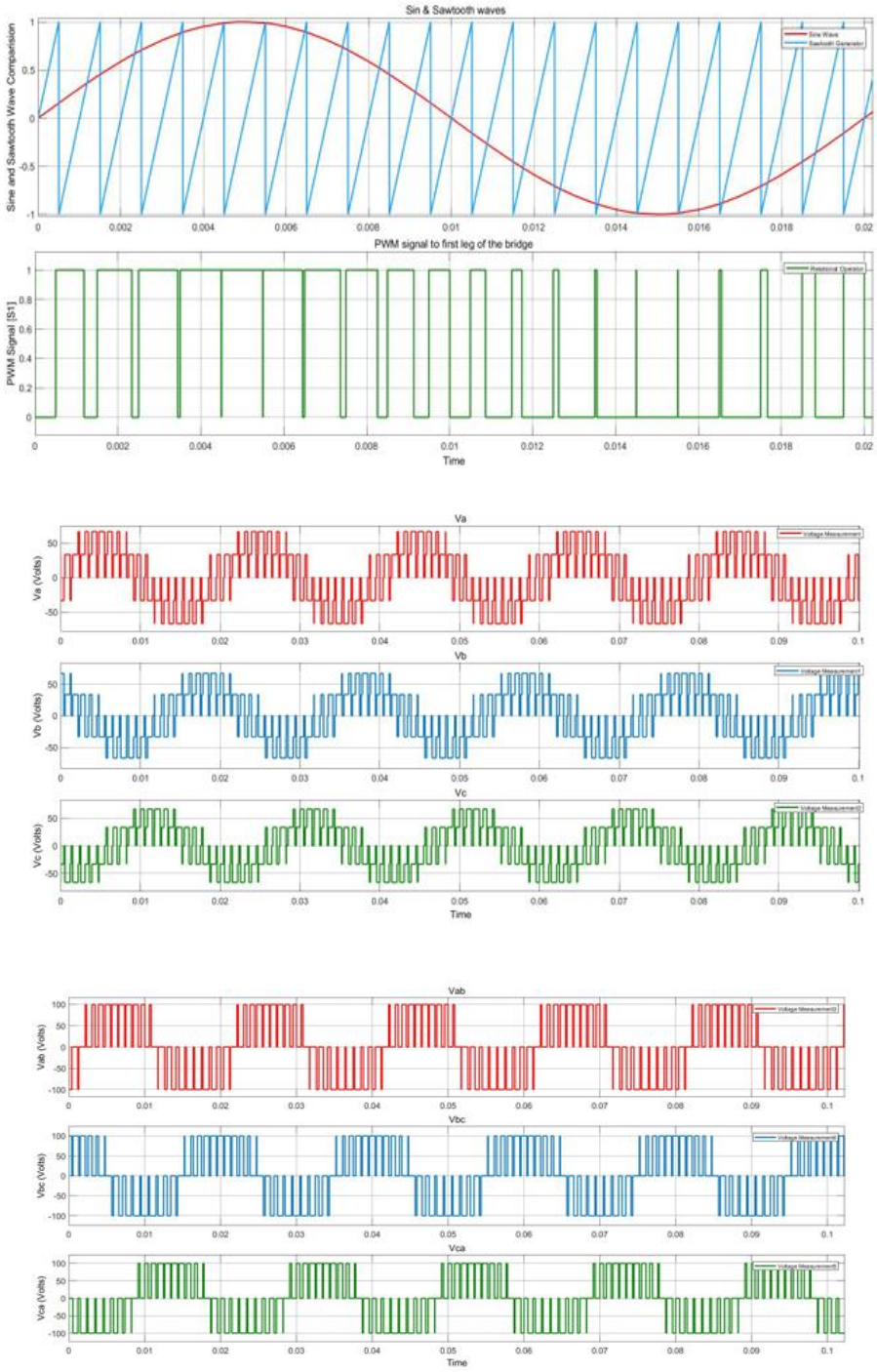

Figure 4: Three-Phase PWM Inverter Input and Output Waveforms

Three-panel plot: (top) Sine vs sawtooth comparison and resulting PWM gate signal S1 over 0–0.02s; (middle) Three output phase voltages Va, Vb, Vc (±50V PWM bursts) over 0–0.1s; (bottom) Three line voltages Vab, Vbc, Vca (±100V) over 0–0.1s, showing characteristic PWM switching pattern

4.3 DC-DC Converter Results for LDV and HDV

Table 1 summarizes the key simulation parameters and measured results for both the LDV (3.3 kW) and HDV (22 kW) DC/DC converter configurations. The LDV converter uses a 24 V nominal battery with a 48 V DC source, while the HDV converter interfaces with a three-phase 415 V AC supply. Both configurations demonstrate successful bidirectional operation with the battery SOC responding appropriately to charging and discharging commands.

Parameter	LDV Converter (3.3 kW)	HDV Converter (22 kW)
Battery Nominal Voltage	24 V	24 V
DC Source Voltage	48 V	415 V (line, AC)
Rated Capacity	10 Ah	10 Ah
Switching Frequency	10 kHz	10 kHz
SOC Initial / Charging / Discharging	50% / 50.24% / 49.98%	50% / 50.08%
Charging Current (Ib)	-86.88 A	~High transient
Battery Voltage (Vb) Charging	30.62 V	~25 V
Effective Power Rating	3.3 kW	22 kW

Table 1: Simulation Parameters and Results for LDV and HDV DC/DC Converters

Figure 5 shows the LDV converter charging and discharging waveforms. During charging (pulse width = 70%), the battery SOC increases from 50% to 50.24% over 1 second, with a steady charging current of approximately -86.88 A and battery voltage rising to 30.62 V. During discharging (pulse width = 40%), the SOC decreases to 49.98% with a positive current of 9.157 A and voltage settling at 25.34 V.

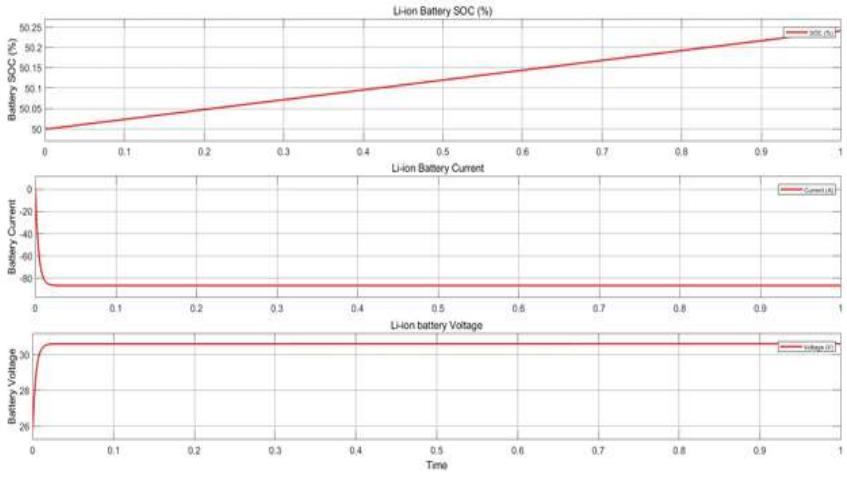

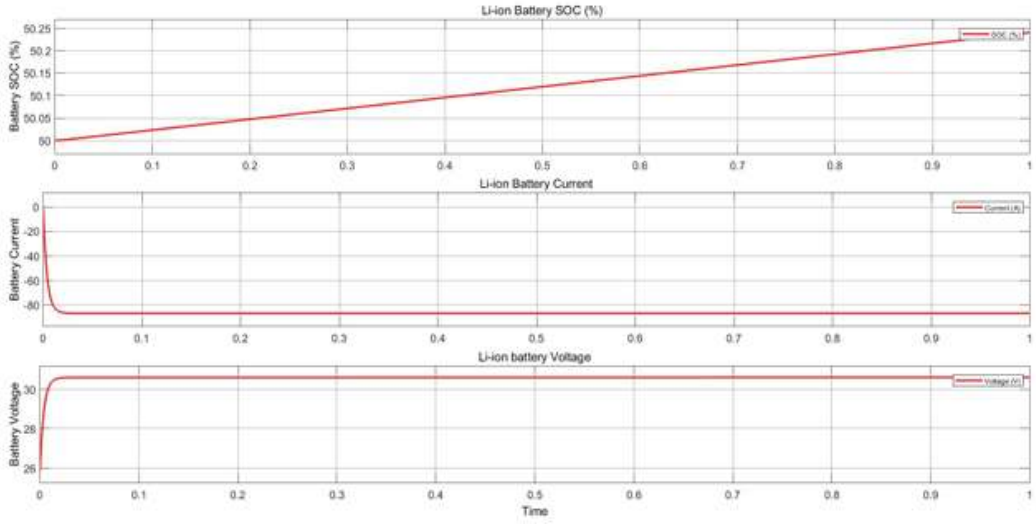

Figure 5: LDV DC/DC Converter: Charging and Discharging Output Waveforms

Six-panel plot (3 charging + 3 discharging): For each mode — (top) Li-ion Battery SOC% (50→50.25% charging; 50→49.98% discharging) over 0–1s; (middle) Battery current (negative ~-80A charging; positive ~9A discharging); (bottom) Battery voltage (26–30V range). Both configurations demonstrate stable, monotonic battery parameter response

4.4 V2G Reverse Charging Validation

The V2G reverse charging topology converts DC battery power to three-phase AC output. Figure 6 demonstrates the dramatic improvement in output voltage quality achieved by the LCL filter. Without the filter, the output exhibits high-frequency PWM switching noise (±40 V spikes). With the 5mH-30µF-5mH LCL filter applied, the three-phase output voltages Va, Vb, and Vc display clean sinusoidal waveforms at approximately ±30 V peak, suitable for grid injection.

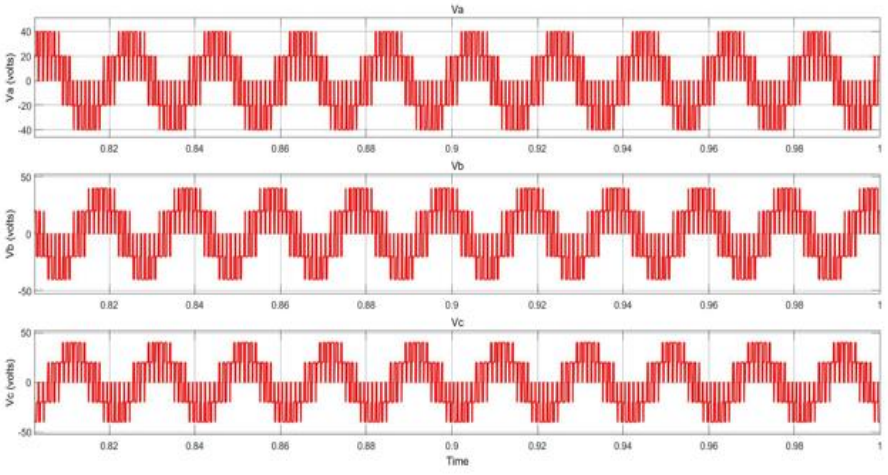

Figure 6: V2G Output Phase Voltages: Without and With LCL Filter

4.5 Autonomous V2G-G2V Toggle Switch Operation

The autonomous V2G-G2V system with PLL control was validated under three operating scenarios: steady V2G, steady G2V, and abrupt mode transition. Table 2 summarizes the key performance parameters measured at t = 0.505 s.

Performance Parameter	V2G Mode	G2V Mode
Grid Phase Voltage (Va)	339 V	338.974 V
Grid Phase Current (Ia)	23.081 A	-22.967 A
Active Power (P)	11.31 kW	-11.69 kW
Reactive Power (Q)	172 kVAr	-92.53 kVAr
DC-Link Voltage (Vdc)	800.1 V	799.9 V
Battery Current (Ibat)	30.50 A	-29.52 A
Battery Voltage (Vbat)	387.0 V	388.5 V
Battery SOC Status	Decreasing	Increasing

Table 2: Performance Parameters of V2G and G2V Modes at t = 0.505 s

In V2G mode (Figure 7a), the battery SOC decreases linearly from 50% as energy is extracted, while the grid voltage and current waveforms are in phase (0° phase difference), confirming active power injection into the grid. The DC-link voltage exhibits an initial transient reaching 835 V before settling at the reference value of 800 V within approximately 0.3 s.

In G2V mode (Figure 7b), the battery SOC increases, and the grid current is 180° out of phase with the grid voltage, confirming power absorption from the grid. The DC-link voltage settles at 800 V from an initial undershoot of 765 V.

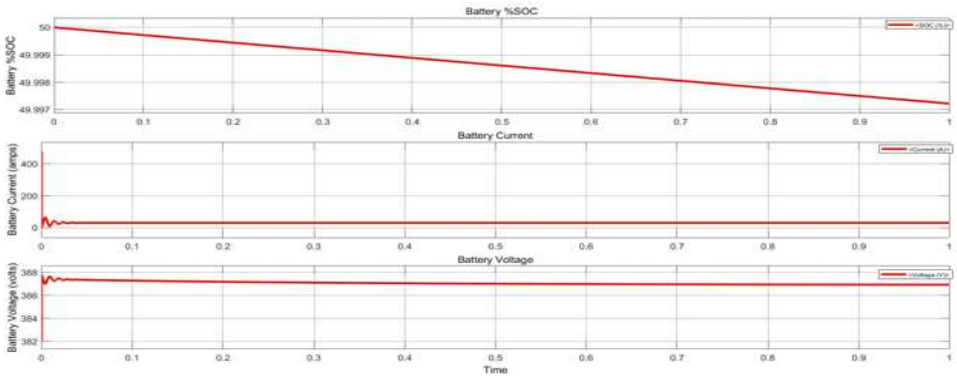

(a1)

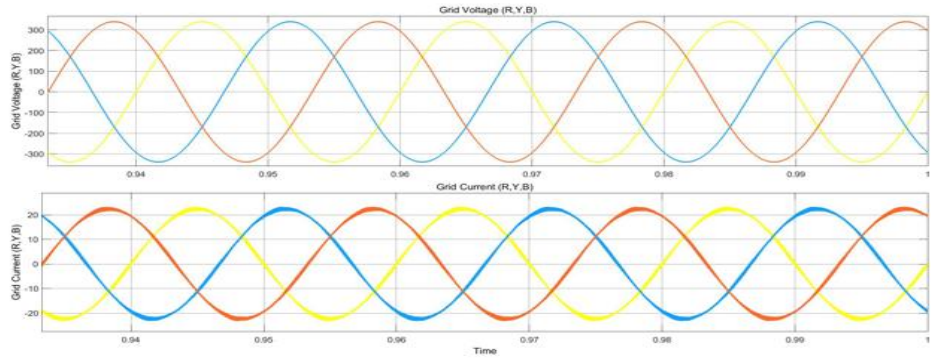

(a2)

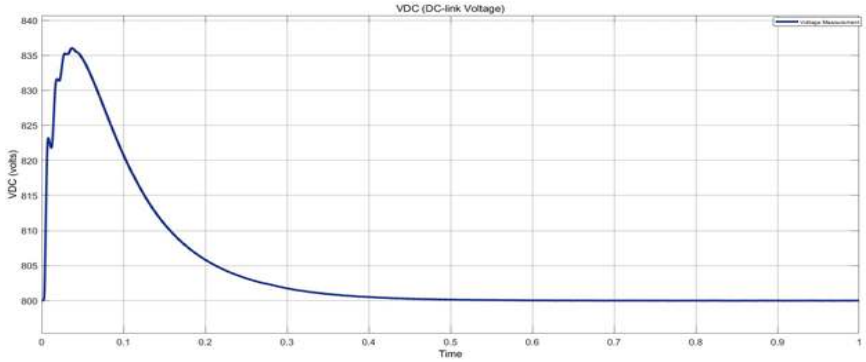

(a3)

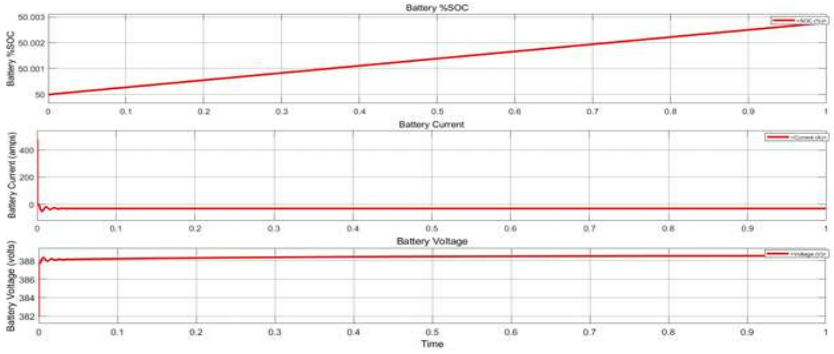

(b1)

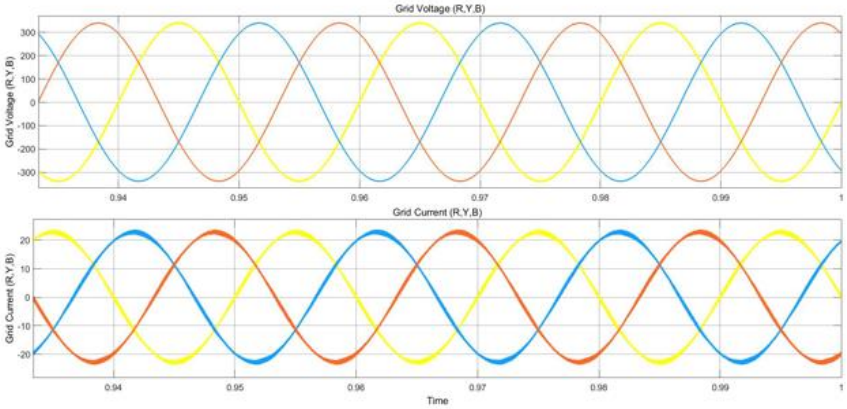

(b2)

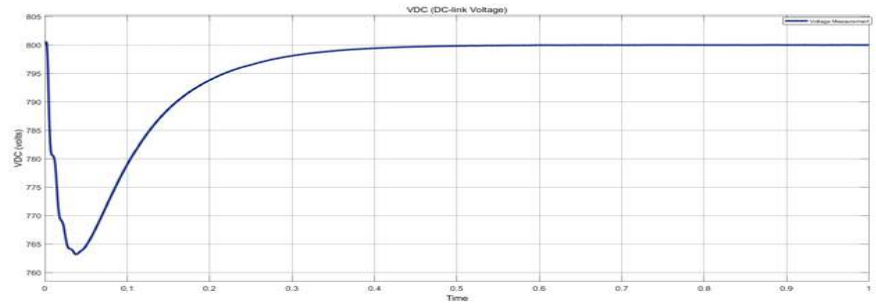

(b3)

Figure 7: Autonomous V2G and G2V Mode Operation Results

Six-panel display (3 per mode): V2G Mode — (a1) Battery %SOC decreasing 50→49.997%, current ~30A, voltage 382–388V over 0–1s; (a2) Three-phase grid voltages (R/Y/B, ±300V) and currents (±20A) IN PHASE confirming V2G; (a3) DC-link voltage transient: peak 835V → settling at 800V. G2V Mode — (b1) Battery %SOC increasing 50→50.003%, current settling ~0A; (b2) Grid voltage and current 180° OUT OF PHASE confirming G2V; (b3) DC-link voltage rising from 765V → stabilizing at 800V

4.6 Abrupt Mode Transition Performance

A critical test of the control system is its response to abrupt mode switching. Figure 8 shows the system behavior when the operating mode is changed from V2G to G2V at t = 0.5 s. The PLL controller re-synchronizes the phase relationship within approximately 2-3 grid cycles (~40-60 ms). The DC-link voltage exhibits a transient dip to approximately 725 V before recovering to 800 V, while the battery current smoothly reverses polarity. This rapid response demonstrates the effectiveness of the PLL control architecture for real-world smart grid applications where demand conditions may change rapidly.

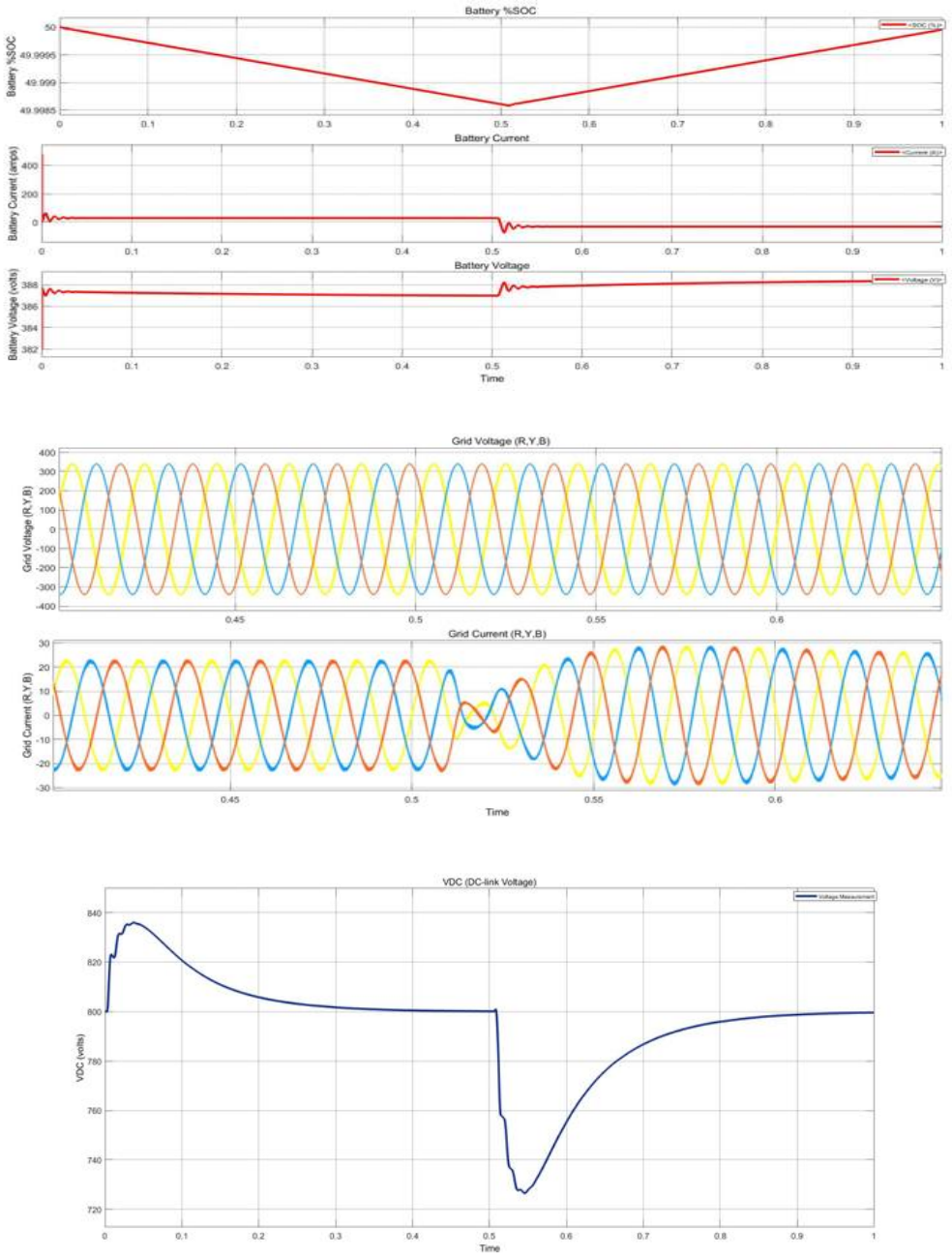

Figure 8: System Response During Abrupt V2G to G2V Mode Transition at t = 0.5 s

Three-panel plot: (top) Battery %SOC showing V-shape: decreasing in V2G (49.9985%) then increasing after switch at t=0.5s in G2V mode; (middle) Grid voltage (±400V) and current (±30A) — current reverses phase from 0° to 180° relative to voltage near t=0.5s; (bottom) DC-link voltage showing initial stability at ~800V, then sharp dip to ~725V at mode switch, recovering to 800V by t=0.7s — all plotted 0.3 to 0.65 second window.

4.7 Parallel Battery Operation

Expanding the system to parallel battery operation (simulating multiple EVs connected simultaneously) yields significant improvements in both power capacity and harmonic performance. Table 3 compares key metrics between single and parallel battery configurations.

Metric	Single Battery	Parallel Batteries
Grid Current THD (%)	2.45%	0.93%
Fundamental Current (50 Hz)	22.36 A	67.14 A
DC-link Voltage Peak (V2G)	~835 V	~900 V
DC-link Steady State	800 V	800 V
IEEE 519 THD Limit	5%	5%
Compliance	Yes (51% margin)	Yes (81% margin)

Table 3: THD Comparison: Single vs. Parallel Battery V2G-G2V Operation

With parallel battery operation, the grid current fundamental component increases from 22.36 A to 67.14 A, reflecting the higher aggregate power capacity. More significantly, the grid current THD improves dramatically from 2.45% to 0.93% (Figure 9). This improvement results from the effective cancellation of switching harmonics between the parallel converter units, analogous to an interleaved converter effect. Both values comfortably satisfy the IEEE 519 standard requirement of THD < 5%.

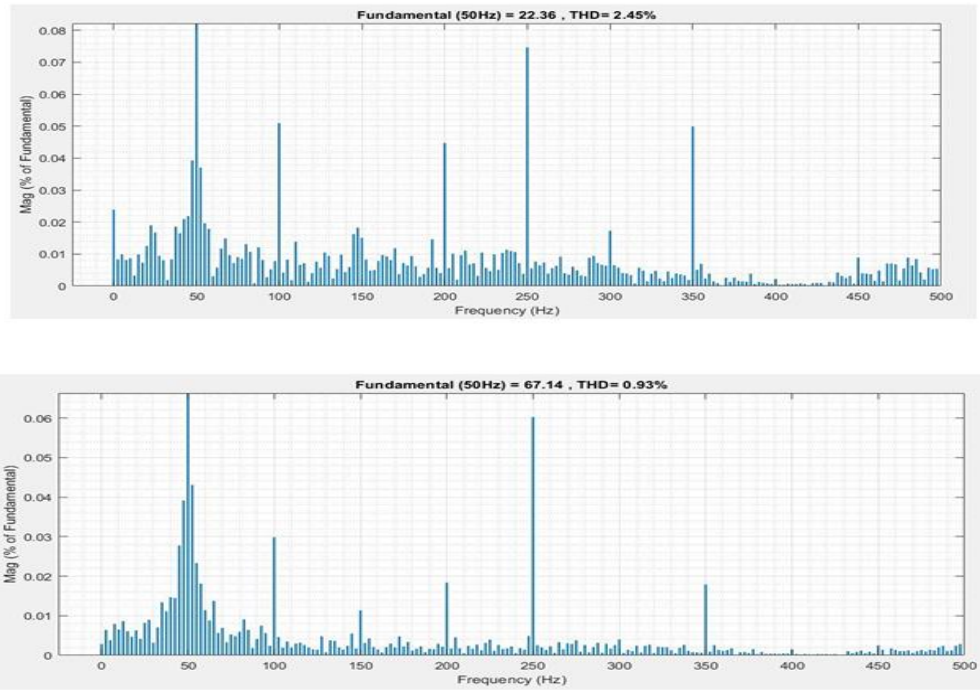

Figure 9: FFT Analysis: THD Comparison for Single vs. Parallel Battery Operation

Two-panel FFT spectrum plot: (left) Single battery — Fundamental(50Hz) = 22.36A, THD = 2.45%; magnitude spectrum 0–500Hz showing harmonic peaks mainly at 150Hz, 250Hz bands (0–0.08 per-unit). (right) Parallel batteries — Fundamental(50Hz) = 67.14A, THD = 0.93%; same frequency axis showing significantly reduced harmonic magnitudes (0–0.06 per-unit) confirming improved harmonic cancellation with parallel EV operation.

CONCLUSION

This paper has presented a comprehensive design and simulation study of bidirectional power converter topologies for V2G and G2V applications. The proposed system, implemented in MATLAB/Simulink, demonstrates successful autonomous bidirectional power flow control through a PLL-based strategy without manual intervention. Key findings are summarized as follows:

The three-phase full-bridge and PWM inverter topologies provide effective AC/DC and DC/AC conversion as the grid interface stages. The LCL filter (5mH-30μF-5mH) is essential for achieving acceptable grid-side waveform quality in V2G mode. The PLL controller achieves rapid synchronization (within ~50 ms) under both steady-state and abrupt mode transition conditions, confirming its suitability for real smart grid deployments.

The system achieves THD values of 2.45% (single battery) and 0.93% (parallel batteries), both significantly below the IEEE 519 standard limit of 5%. The parallel battery configuration not only increases power capacity proportionally but also provides inherent harmonic cancellation, making it an attractive architecture for large-scale EV aggregation scenarios.

Active power of approximately 11.5 kW is successfully transferred in both V2G and G2V modes with stable DC-link voltage regulation at 800 V. The proposed transformerless topology reduces cost and losses compared to isolation-transformer-based alternatives, making it commercially viable.

Future work should explore integration with renewable energy sources such as photovoltaic arrays, implementation of advanced predictive control algorithms, and hardware-in-the-loop (HIL) validation. The incorporation of cyber-physical systems (CPS) for remote monitoring and control, along with standardized communication protocols (e.g., ISO 15118), will be essential for commercial deployment. Development of monetization frameworks that incentivize EV owners to participate in grid services represents a critical non-technical challenge that warrants interdisciplinary research.

REFERENCES

1. Z. Zhang, B. Liu and S. Song, "Power Decoupling Control for V2G/G2V/PV2G Operation Modes in Single-Phase PV/Battery Hybrid Energy System With Low DC-Link Capacitance," IEEE Access, vol. 9, pp. 160975-160986, 2021.
2. M. A. Islam et al., "Modeling and Performance Evaluation of ANFIS Controller-Based Bidirectional Power Management Scheme in Plug-In Electric Vehicles Integrated With Electric Grid," IEEE Access, vol. 9, pp. 166762-166780, 2021.
3. B. Chelladurai, C. K. Sundarabalan, S. N. Santhanam and J. M. Guerrero, "Interval Type-2 Fuzzy Logic Controlled Shunt Converter Coupled Novel High-Quality Charging Scheme for Electric Vehicles," IEEE Trans. Ind. Inform., vol. 17, no. 9, pp. 6084-6093, 2021.
4. A. K. Seth and M. Singh, "Second-Order Ripple Minimization in Single-Phase Single-Stage Onboard PEV Charger," IEEE Trans. Transp. Electrif., vol. 7, no. 3, pp. 1186-1195, 2021.
5. H.-C. Chen and B.-W. Huang, "Integrated G2V/V2G Switched Reluctance Motor Drive With Sensing Only Switch-Bus Current," IEEE Trans. Power Electron., vol. 36, no. 8, pp. 9372-9381, 2021.
6. S. H. Hosseini, R. Ghazi and H. Heydari-Doostabad, "An Extendable Quadratic Bidirectional DC-DC Converter for V2G and G2V Applications," IEEE Trans. Ind. Electron., vol. 68, no. 6, pp. 4859-4869, 2021.
7. A. Verma and B. Singh, "AFF-SOGI-DRC Control of Renewable Energy Based Grid Interactive Charging Station for EV With Power Quality Improvement," IEEE Trans. Ind. Appl., vol. 57, no. 1, pp. 588-597, 2021.
8. J.-J. Kao et al., "Adaptive Bidirectional Inductive Power and Data Transmission System," IEEE

Trans. Power Electron., vol. 36, no. 7, pp. 7550-7563, 2021.

9. K. P. Inala, B. Sah, P. Kumar and S. K. Bose, "Impact of V2G Communication on Grid Node Voltage at Charging Station in a Smart Grid Scenario," IEEE Syst. J., vol. 15, no. 3, pp. 3749-3758, 2021.
10. G. Guru Kumar and S. Kumaravel, "Dual-Input Non-isolated DC-DC Converter with Vehicle to Grid Feature," IEEE J. Emerg. Sel. Topics Power Electron., 2021.
11. H. Heydari-doostabad and T. O'Donnell, "A Wide-Range High-Voltage-Gain Bidirectional DC-DC Converter for V2G and G2V Hybrid EV Charger," IEEE Trans. Ind. Electron., vol. 69, no. 5, pp. 4718-4729, 2022.
12. K. Sarita et al., "Power Enhancement With Grid Stabilization of Renewable Energy-Based Generation System Using UPQC-FLC-EVA Technique," IEEE Access, vol. 8, pp. 207443-207464, 2020.
13. H. M. Khalid and J. C. H. Peng, "Bidirectional Charging in V2G Systems: An In-Cell Variation Analysis of Vehicle Batteries," IEEE Syst. J., vol. 14, no. 3, pp. 3665-3675, 2020.
14. S. Taghizadeh et al., "A Multifunctional Single-Phase EV On-Board Charger With a New V2V Charging Assistance Capability," IEEE Access, vol. 8, pp. 116812-116823, 2020.
15. S. Liu et al., "A Hierarchical V2G/G2V Energy Management System for Electric-Drive-Reconstructed Onboard Converter," IEEE Access, vol. 8, pp. 198201-198213, 2020.
16. R. Sharma and H. Sharma, "Deep Reinforcement Learning-Based Smart Charging of Electric Vehicles in V2G Framework," IEEE Trans. Smart Grid, vol. 13, no. 4, pp. 3080-3092, 2022.
17. A. Ul-Haq, M. Cecati and E. El-Saadany, "Probabilistic Modeling of Electric Vehicle Charging Pattern in a Residential Distribution Network," Electric Power Systems Research, vol. 157, pp. 126-133, 2022.
18. T. Dragicevic, S. Vazquez and P. Wheeler, "Advanced Control Methods for Power Converters in DG Systems and Microgrids," IEEE Trans. Ind. Electron., vol. 68, no. 7, pp. 5847-5852, 2021.
19. M. C. Kisacikoglu, A. Bhatt, R. Garcia and W. Soong, "Single-Phase On-Board Bidirectional PEV Charger for V2G Reactive Power Operation," IEEE Trans. Smart Grid, vol. 6, no. 2, pp. 767-775, 2021.
20. E. Chemali, P. J. Kollmeyer, M. Preindl, R. Ahmed and A. Emadi, "Long Short-Term Memory Networks for Accurate

HOW TO CITE: Poornima S. Kamkar*[1], Sreenath K.[1], H. A. Shruti[1], Chandan N. J.[2], Pradeep N.[2], Bidirectional Power Converter Topologies For V2G And G2V Integration In Smart Grid Systems: Design, Control, And Performance Evaluation, Int. J. Sci. R. Tech., 2026, 3 (5), 1134-1146. https://doi.org/10.5281/zenodo.20445677